Supporting information

Insight into a complexation mechanism between $BiVO_4$ photoanode and tartaric acid for efficient photoelectrochemical H_2 production

Zhaoqi Wang[a], Shuhua Wang[b], Xiaolei Liu[a,*], Yayang Xu[a], Dujuan Dai[a], Shuang Zhao[a], Peng Wang[a], Zhaoke Zheng[a], Yuanyuan Liu[a], Hefeng Cheng[a], Ying Dai[b], Zeyan Wang[a,*], Baibiao Huang[a,*]

[a] State Key Laboratory of Crystal Materials, Shandong University, Jinan 250100, China

[b] School of Physics, Shandong University, Jinan 250100, China

*Corresponding authors' e-mail addresses: liuxiaolei@sdu.edu.cn (X. Liu); wangzeyan@sdu.edu.cn (Z. Wang); bbhuang@sdu.edu.cn (B. Huang)

Experimental section

Fabrication of ZnO photoanode

The ZnO photoanode was synthesized using a hydrothermal method.[1] First, 0.44 g of zinc nitrate hexahydrate and 0.22 g of hexamethylenetetramine was dissolved in 60 ml of water and transferred to a 100 ml autoclave. An FTO glass substrate with an Al foil-covered edge was inserted into the autoclave with its conducting surface facing downwards. The autoclave was maintained at 90 °C for 4 h and cooled down naturally. The resulting photoanode was rinsed with water and ethanol before being left to dry overnight. The final product was a ZnO photoanode.

Fabrication of TiO_2 photoanode

The TiO_2 photoanode was prepared using a hydrothermal method, as described in previous studies.[2] In brief, a white solution containing 30 ml of hydrochloric acid, 30 ml of water, and 1.0 ml of titanium n-butoxide was transferred into a autoclave along with an FTO glass (conducting surface down). The autoclave was then maintained at 150 °C for 5 h, followed by a natural cooling process. The resulting sample was rinsed with water and dried, and subsequently annealed at 550 °C for 4 h. Finally, the TiO_2 photoanode was obtained.

Fabrication of WO_3 photoanode

The WO_3 photoanode was synthesized via a hydrothermal and annealing process.[3] Initially, 0.5 g of sodium tungstate dihydrate was dissolved in 60 ml of water and vigorously stirred. Next, 12 ml of 3.0 M hydrochloric acid and 0.4 g of ammonium oxalate were added to the solution and stirred vigorously again. The resulting solution was transferred to a 100 ml autoclave containing an upside-down FTO substrate. The autoclave was then heated to 120 °C for 12 h before being allowed to cool naturally. The obtained product was rinsed with water and dried at 60 °C for 5 h. The sample was then annealed at 500 °C for 1 h. Finally, the WO_3 photoanode was finally obtained after cooling the sample.

Characterizations

The structures and morphologies of the prepared photoanodes were characterized using X-ray diffraction (XRD, Bruker D8-Advance) and scanning electron microscopy (SEM, Hitachi S-4800). Ultraviolet-visible diffuse reflectance spectroscopy (UV-Vis DRS) measurements of the photoanodes were performed by a UV-vis spectrophotometer (Shimadzu 2550) equipped with an integrating sphere, with $BaSO_4$ serving as the reference material. The elements chemical states and chemical environment of the prepared photoanodes were determined by X-ray photoelectron spectroscopy (XPS, Thermo Fisher Scientific Escalab Xi+) using a monochromatic Al-Kα source. The C1s peak at 284.8 eV was used to calibrated the peak positions of the measured elements.

Calculation details

The first-principles density functional theory (DFT) simulations were performed utilizing Viennna *ab initio* simulation package with the generalized gradient approximation (GGA) and Perdew-Burke-Ernzerhof (PBE) exchange-correlation function.[4-6] To illustrate the interaction between valence electrons and ionic cores, the projected augmented wave (PAW) potentials with a plane wave basis set were adopted, while the kinetic cut-off energy was set to 450 eV.[7, 8] To determine the partial occupancies of Kohn-Sham orbitals, the Gaussian smearing method with a width of 0.05 eV were used. The electronic energy was reckoned as self-consistent under the condition that the energy change is within 10^{-5} eV and the geometry optimization of atomic structure was reckoned as convergent under the condition that the energy change is within 0.05 eV $Å^{-1}$. The vacuum spacing is 20 Å for the surface system in the direction that perpendicular to plane. The Brillouin zone integration were performed by a 4×5×1 k-points sampling under the Monkhorst-Pack scheme. And the adsorption energy (E_{ad}) were calculated by the follow equation:

$$E_{ads} = E_{ad-sub} - E_{ad} - E_{sub}$$

Where E_{ad-sub} is the total energy of the optimized system, E_{ad} is the energy of adsorbate and the E_{sub} is the energy of substrate.

Supplementary data

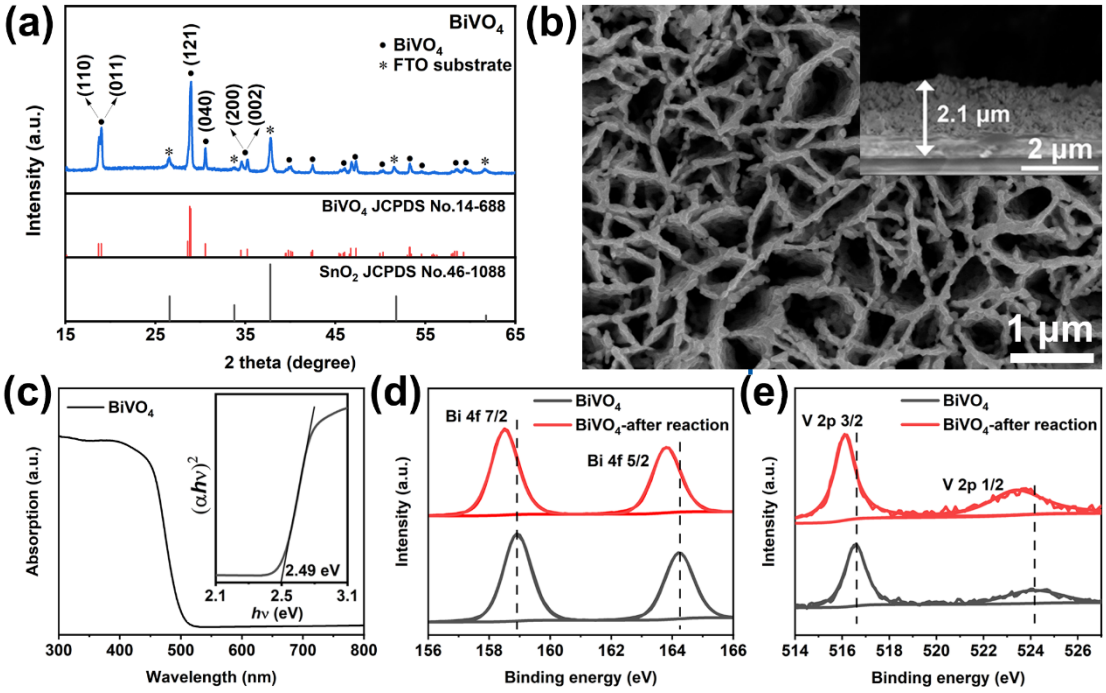

Fig. S1 (a) XRD pattern, (b) top and the inserted cross-sectional view SEM images, (c) UV-Vis DRS spectrum and the inserted Tauc-plot of the $BiVO_4$ photoanode. (d) Bi 4f and (e) V 2p XPS peaks of the $BiVO_4$ photoanode before and after the PEC test in KPi + 0.5 M $C_4H_6O_6$ solution.

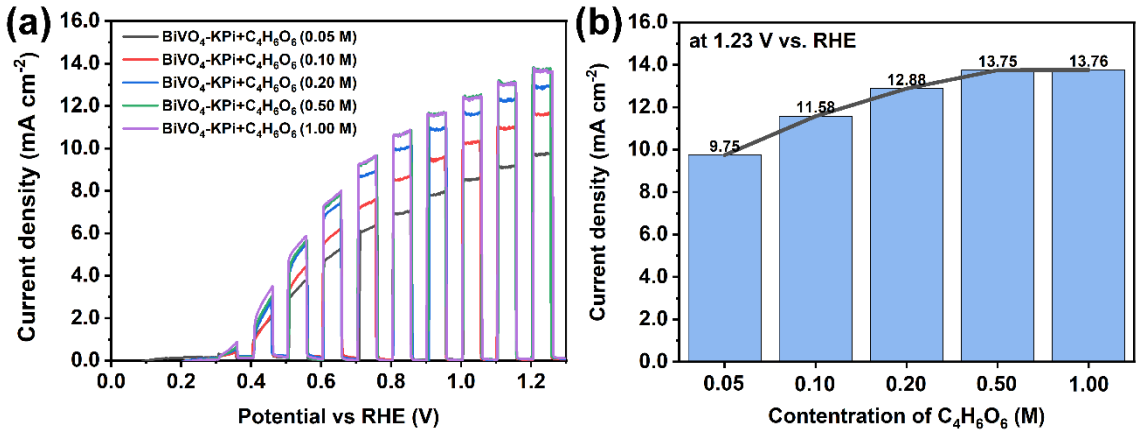

Fig. S2 (a) Current density-potential (J-p) curves of the $BiVO_4$ photoanode under AM 1.5 G irradiation or in the dark in KPi + $C_4H_6O_6$ solution with different concentrations of $C_4H_6O_6$. (b) Current density of the $BiVO_4$ photoanode at 1.23 V versus RHE in KPi + 0.5 M $C_4H_6O_6$ solution with different concentrations of $C_4H_6O_6$.

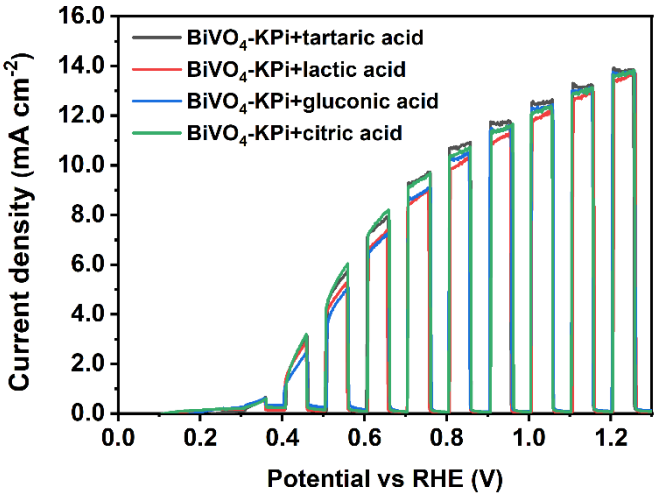

Fig. S3 J-p curves of the $BiVO_4$ photoanode under AM 1.5 G irradiation or in the dark in KPi + 0.5 M tartaric acid ($C_4H_6O_6$), KPi + 0.5 M lactic acid, KPi + 0.5 M gluconic acid, and KPi + 0.5 M citric acid solutions.

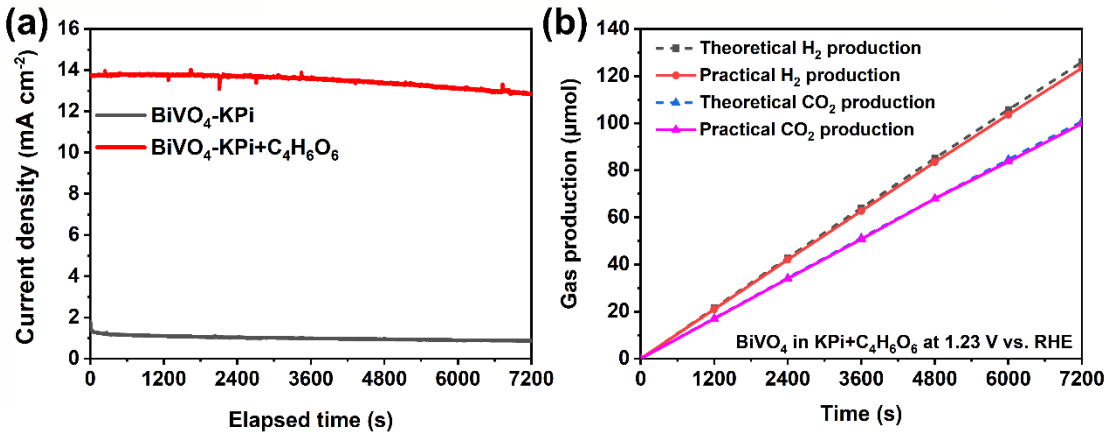

Fig. S4 (a) Current density-time (J-t) curves of the $BiVO_4$ photoanode measured at 1.23 V versus RHE in KPi and KPi + 0.5 M $C_4H_6O_6$ solutions. (b) Theoretical and practical H_2 and CO_2 production of the $BiVO_4$ photoanode measured at 1.23 V versus RHE in KPi + 0.5 M $C_4H_6O_6$ solution.

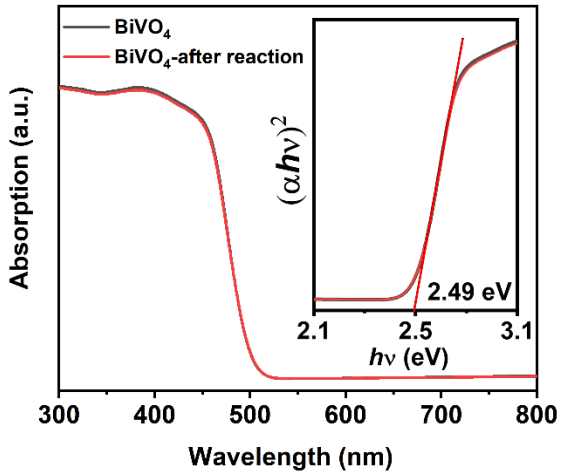

Fig. S5 UV-vis DRS spectrum and the inserted Tauc-plot of the $BiVO_4$ photoanode before and after the PEC test in KPi + 0.5 M $C_4H_6O_6$ solution.

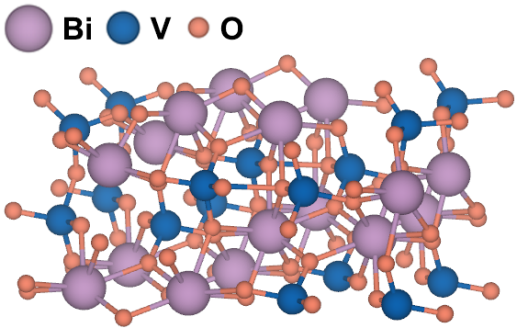

Fig. S6 Simulated structure of the $BiVO_4$ (121) surface after geometric optimization (the purple, blue and orange spheres represent Bi, V, and O atoms in turn).

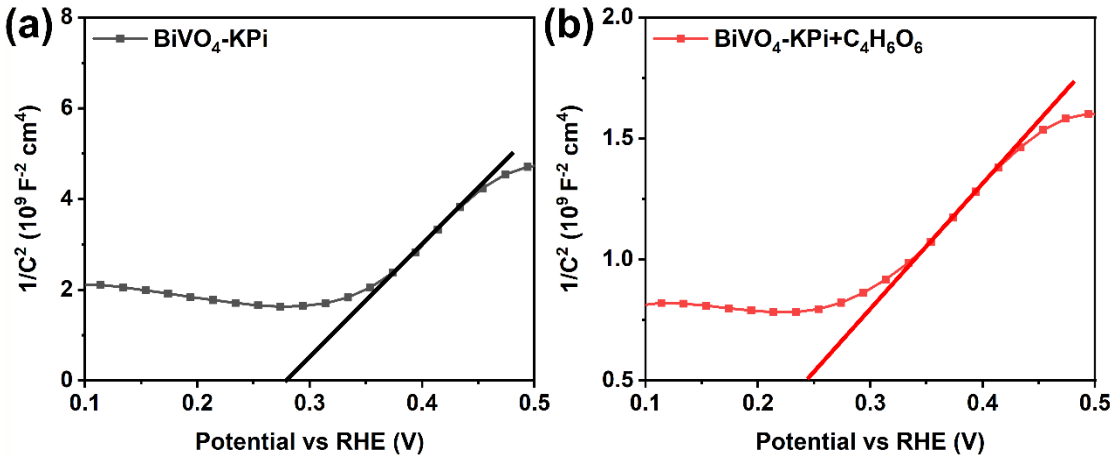

Fig. S7 Mott-Schottky plots of the $BiVO_4$ photoanode in (a) KPi and (b) KPi + 0.5 M $C_4H_6O_6$ solutions.

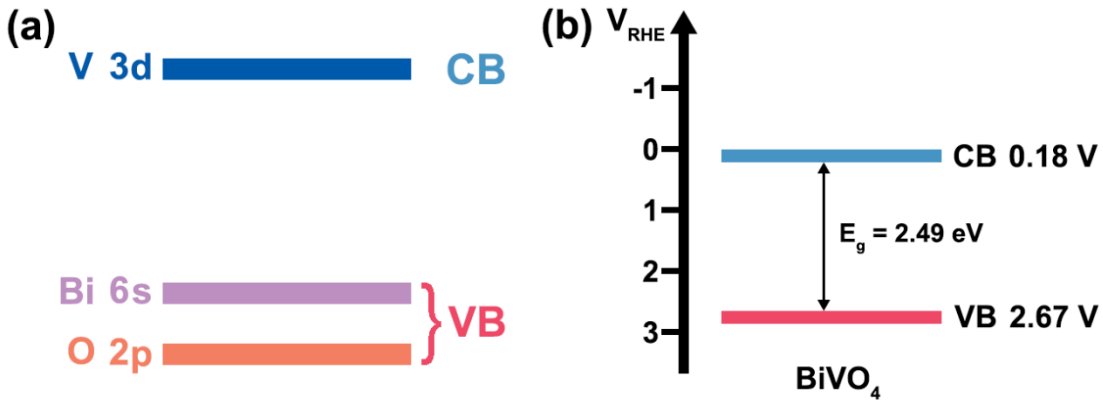

Fig. S8 Schematic diagram of (a) the band structure and (b) the band positions of $BiVO_4$.

In the case of an n-type semiconductor, it is generally accepted that the flat band potential obtained by Mott-Schottky measurement is assumed to be situated at approximately 0.1 eV below the CB.[1] The flat band potential of $BiVO_4$ photoanode obtained from Mott-Schottky measurement is 0.28 V vs. RHE. Therefore, the CB position of $BiVO_4$ is calculated to be 0.18 V vs. RHE. Moreover, the bandgap of $BiVO_4$ obtained by Tauc-plot is 2.49 eV. Finally, the VB position of $BiVO_4$ is determined to be 2.67 V vs. RHE.

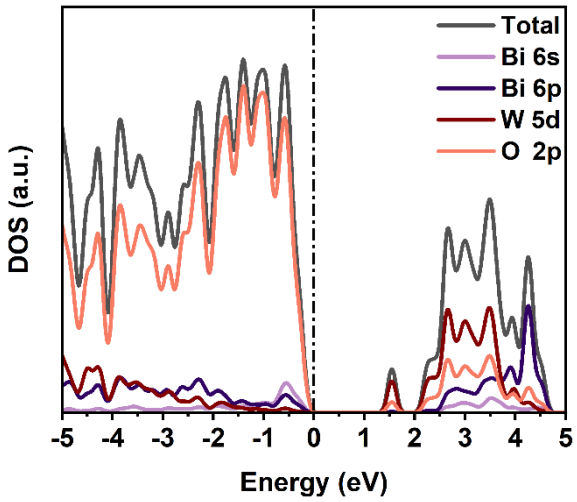

Fig. S9 (a) Total DOS (TDOS) and partial DOS (PDOS) of Bi_2WO_6.

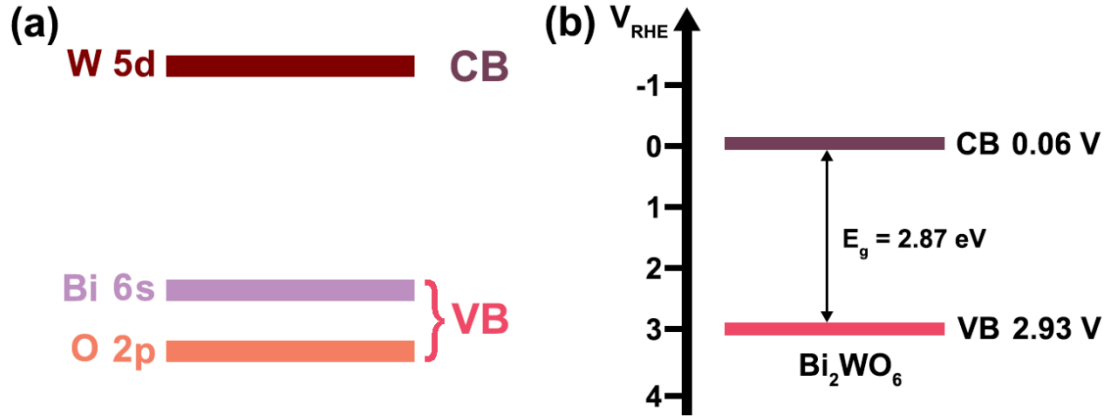

Fig. S10 Schematic diagram of (a) the band structure and (b) the band positions of Bi_2WO_6.

The flat band potential of Bi_2WO_6 photoanode obtained from Mott-Schottky measurement is 0.16 V vs. RHE. Therefore, the CB position of Bi_2WO_6 is calculated to be 0.06 V vs. RHE. Moreover, the bandgap of Bi_2WO_6 obtained by Tauc-plot is 2.87 eV. Finally, the VB position of Bi_2WO_6 is determined to be 2.93 V vs. RHE.

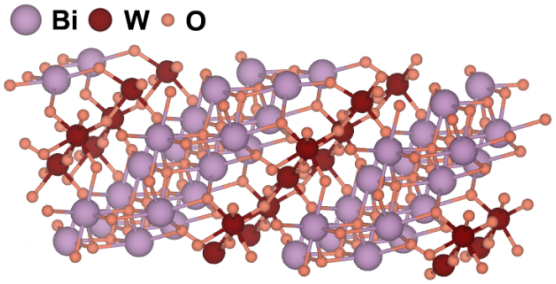

Fig. S11 Simulated structure of the Bi_2WO_6 (026) surface after geometric optimization (the purple, crimson, and orange spheres represent Bi, W, and O atoms in turn).

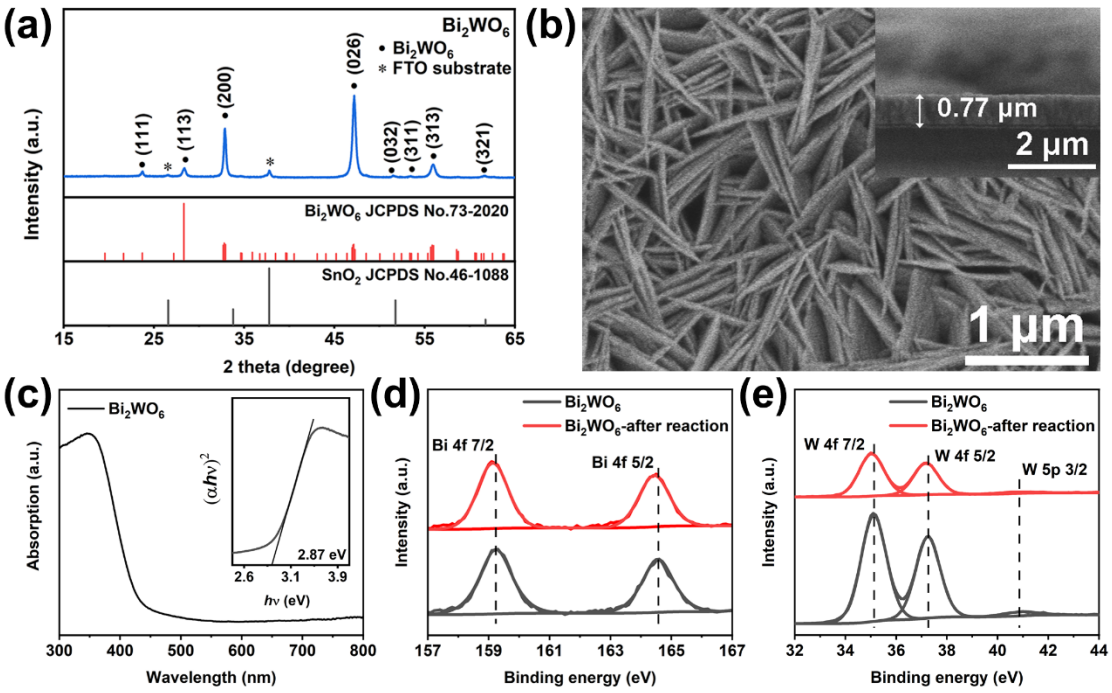

Fig. S12 (a) XRD pattern, (b) top and the inserted cross-sectional view SEM images, (c) UV-vis DRS spectrum and the inserted Tauc-plot of the Bi_2WO_6 photoanode. (d) Bi 4f and (e) W 4f and W 5p XPS peaks of the Bi_2WO_6 photoanode before and after the PEC test in KPi + 0.5 M $C_4H_6O_6$ solution.

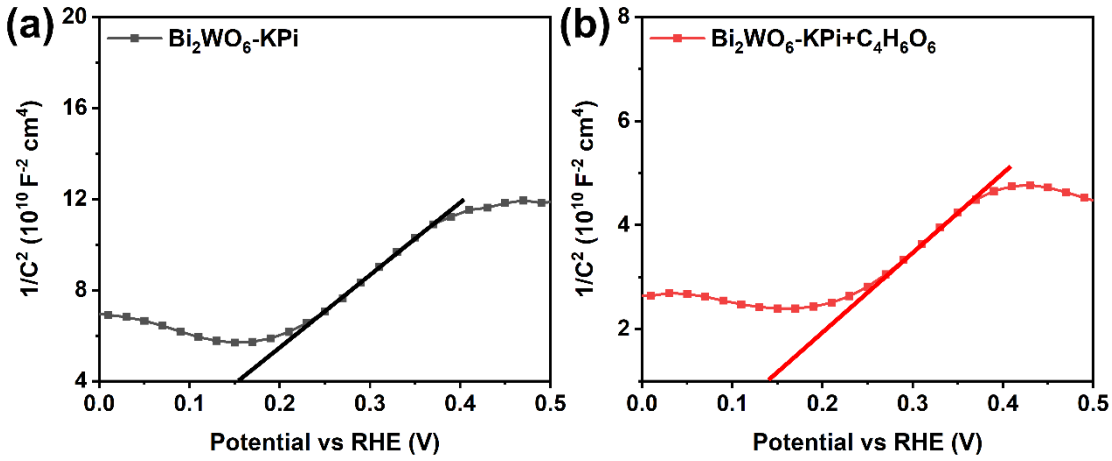

Fig. S13 Mott-Schottky plots of the Bi_2WO_6 photoanode in (a) KPi and (b) KPi + 0.5 M $C_4H_6O_6$ solutions.

The calculated donor densities (N_d) of Bi_2WO_6 photoanode in KPi and KPi + $C_4H_6O_6$ solutions are 8.27×10^{18} and 2.04×10^{19} cm^{-3}, respectively.

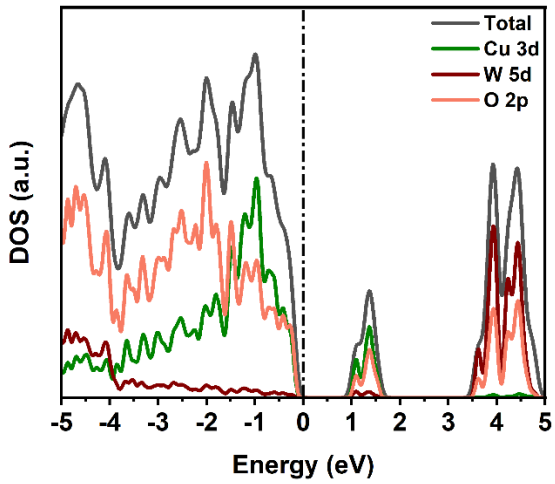

Fig. S14 TDOS and PDOS of $CuWO_4$.

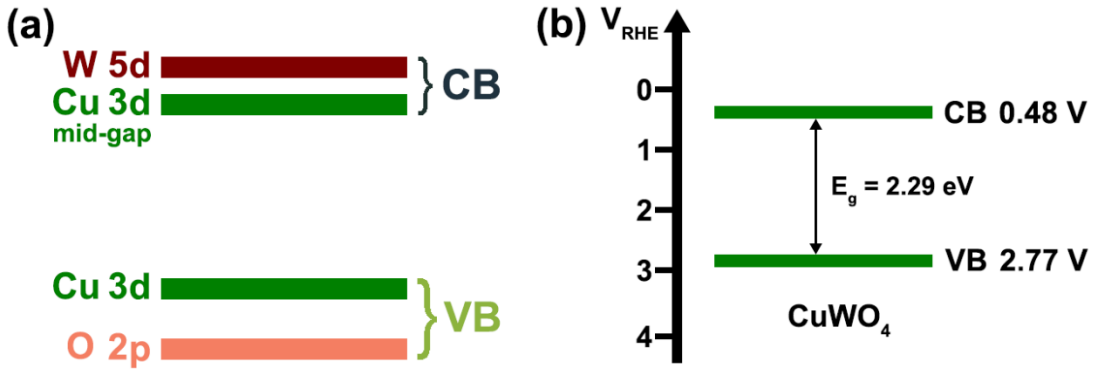

Fig. S15 Schematic diagram of (a) the band structure and (b) the band positions of $CuWO_4$.

The flat band potential of $CuWO_4$ photoanode obtained from Mott-Schottky measurement is 0.58 V vs. RHE. Therefore, the CB position of $CuWO_4$ is calculated to be 0.48 V vs. RHE. Moreover, the bandgap of $CuWO_4$ obtained by Tauc-plot is 2.29 eV. Finally, the VB position of $CuWO_4$ is determined to be 2.77 V vs. RHE.

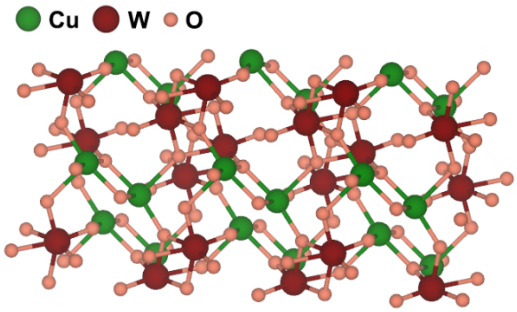

Fig. S16 Simulated structure of the $CuWO_4$ (110) surface after geometric optimization (the green, crimson and orange spheres represent Cu, W, and O atoms in turn).

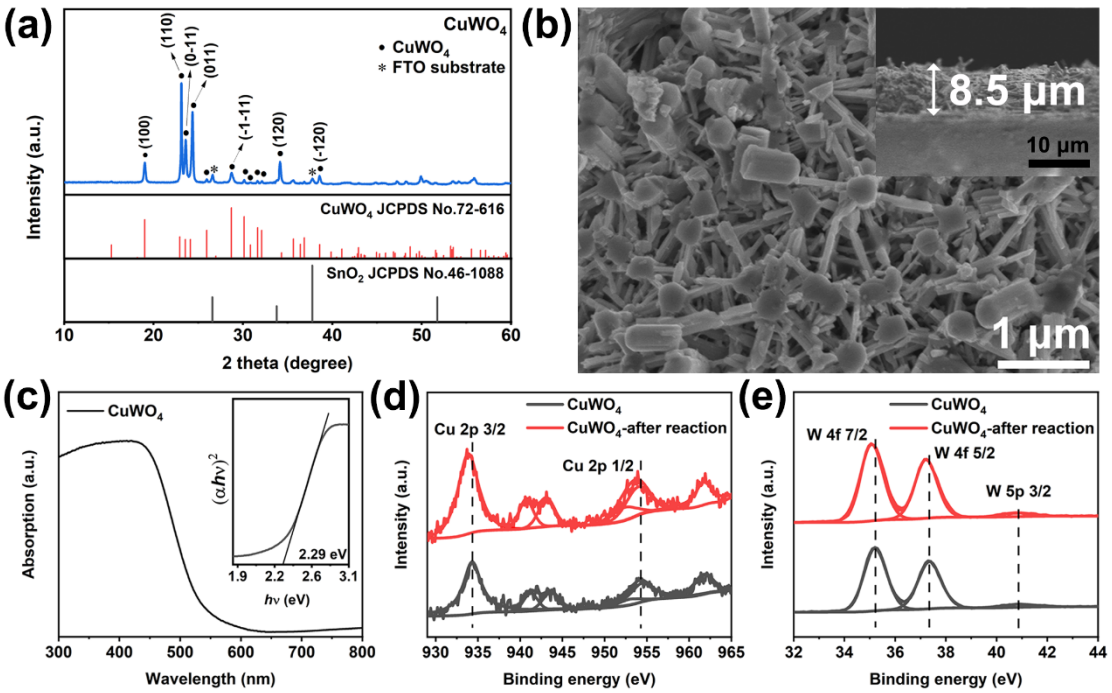

Fig. S17 (a) XRD pattern, (b) top and the inserted cross-sectional view SEM images, (c) UV-vis DRS spectrum and the inserted Tauc-plot of the $CuWO_4$ photoanode. (d) Cu 2p and (e) W 4f and W 5p XPS peaks of the $CuWO_4$ photoanode before and after the PEC test in KPi + 0.5 M $C_4H_6O_6$ solution.

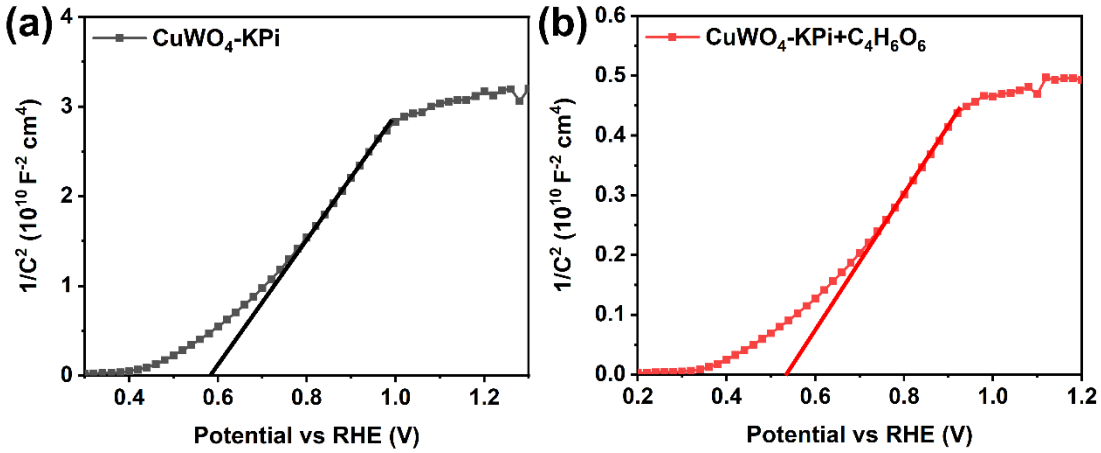

Fig. S18 Mott-Schottky plots of the $CuWO_4$ photoanode in (a) KPi and (b) KPi + 0.5 M $C_4H_6O_6$ solutions.

The calculated N_d for $CuWO_4$ photoanode in KPi and KPi + $C_4H_6O_6$ solutions are 2.30×10^{19} and 1.53×10^{20} cm^{-3}, respectively.

Fig. S19 Schematic diagram of the band structure of ZnO, TiO_2, and WO_3.

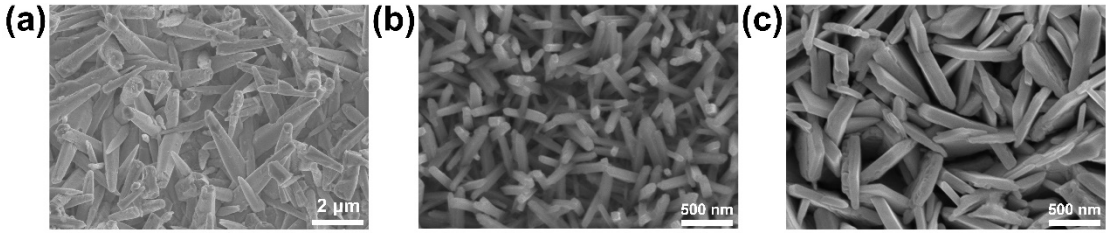

Fig. S20 SEM images of the (a) ZnO, (b) TiO_2, and (c) WO_3 photoanode.

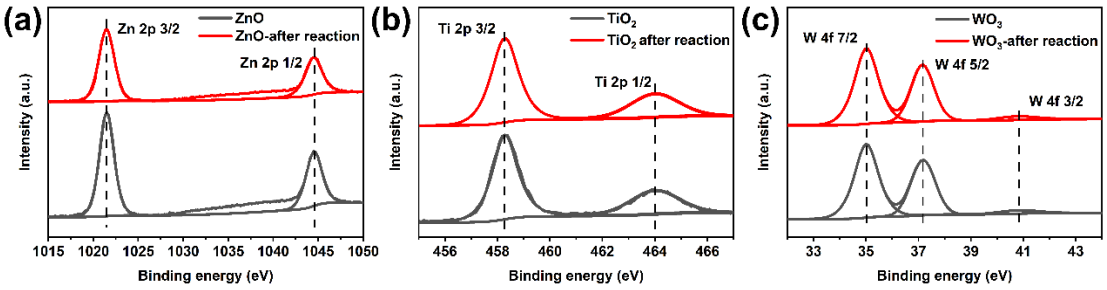

Fig. S21 (a) Zn 2p XPS peaks of the ZnO photoanode, (b) Ti 2p XPS peaks of the TiO_2 photoanode, and (c) W 5p XPS peaks of the WO_3 photoanode before and after the PEC test in KPi + 0.5 M $C_4H_6O_6$ solution.

References

1. Z. K. Zheng, Z. S. Lim, Y. Peng, L. You, L. Chen, J. L. Wang, General route to ZnO nanorod arrays on conducting substrates via galvanic-cell-based approach. *Sci. Rep.,* 2013, **3**, 2434.
2. G. M. Wang, H. Y. Wang, Y. C. Ling, Y. C. Tang, X. Y. Yang, R. C. Fitzmorris, C. C. Wang, J. Z. Zhang, Y. Li, Hydrogen-treated TiO_2 nanowire arrays for photoelectrochemical water splitting. *Nano Lett.,* 2011, **11** (7), 3026-3033.
3. Y. Y. Xu, M. Liu, F. X. Tong, F. H. Ma, X. Y. He, Z. Y. Wang, P. Wang, Y. Y. Liu, H. F. Cheng, Y. Dai, Z. K. Zheng, B. B. Huang, Strain-assisted in-situ formed oxygen defective WO_3 film for photothermal-synergistic reverse water gas shift reaction and single-particle study. *Chem. Eng. J.,* 2022, **433**, 134199.
4. G. Kresse, J. Furthmuller, Efficient iterative schemes for ab initio total-energy calculations using a plane-wave basis set. *Phys. Rev. B,* 1996, **54** (16), 11169-11186.
5. G. Kresse, J. Furthmuller, Efficiency of ab-initio total energy calculations for metals and semiconductors using a plane-wave basis set. *Comput. Mater. Sci,* 1996, **6** (1), 15-50.
6. J. P. Perdew, K. Burke, M. Ernzerhof, Generalized gradient approximation made simple. *Phys. Rev. Lett.,* 1996, **77** (18), 3865-3868.
7. P. E. Blochl, Projector augmented-wave method. *Phys. Rev. B,* 1994, **50** (24), 17953-17979.
8. G. Kresse, D. Joubert, From ultrasoft pseudopotentials to the projector augmented-wave method. *Phys. Rev. B,* 1999, **59** (3), 1758-1775.
9. S. S. Kalanur, Y. J. Lee, H. Seo, A versatile synthesis strategy and band insights of monoclinic clinobisvanite $BiVO_4$ thin films for enhanced photoelectrochemical water splitting activity. *Appl. Surf. Sci.,* 2021, **562**, 150078.